Science of the Total Environment 931 (2024) 172852

Contents lists available at ScienceDirect

Science of the Total Environment

journal homepage: www.elsevier.com/locate/scitotenv

Atmospheric blocking and temperatures in the Antarctic Peninsula

Deniz Bozkurt [a,b,c,d,*], Julio C. Marín [a,b], Cristina Verdugo [b,e], Bradford S. Barrett [f]

[a] Departamento de Meteorología, Universidad de Valparaíso, Chile
[b] Centro de Estudios Atmosféricos y Cambio Climático (CEACC), Universidad de Valparaíso, Chile
[c] Center for Climate and Resilience Research (CR)2, Santiago, Chile
[d] Center for Oceanographic Research COPAS COASTAL, Universidad de Concepción, Chile
[e] Instituto de Física y Astronomía, Universidad de Valparaíso, Chile
[f] Certified Consulting Meteorologist, Raleigh, NC, USA

HIGHLIGHTS

- CMIP6 models and ERA5 show notable differences in historical blocking patterns.
- No consistent trend in future blocking over the Antarctic Peninsula with seasonal model contrasts.
- Extreme blocking conditions cause localized intensification and notable warming in specific regions.
- Improved blocking definitions and a broader mix of climate models are recommended.

GRAPHICAL ABSTRACT

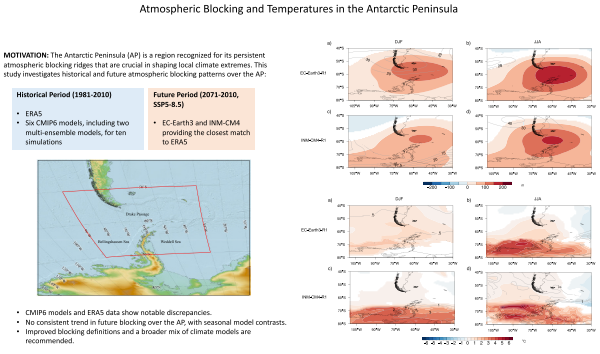

ARTICLE INFO

Keywords:
Climate change
Blocking ridge
CMIP
Model uncertainty
Antarctic Peninsula

ABSTRACT

The Antarctic Peninsula (AP) has displayed a propensity for persistent blocking ridges and anticyclonic conditions, particularly during recent summertime extreme weather events. This study investigates atmospheric blocking patterns over the AP through historical (1981–2010) and future (2071–2100, SSP5–8.5) periods using ERA5 reanalysis and six CMIP6 models, including multi-member realizations from two models totaling ten simulations. We focus particularly on 500 hPa geopotential height (Z500) and near-surface air temperature (T2m) anomalies. The historical analysis highlights significant differences between the CMIP6 models and ERA5 reanalysis, especially in the austral winter, with EC-Earth3 and INM-CM4 models matching closest with the ERA5. Future projections show that while the northern AP and the Drake Passage largely do not exhibit a clear trend towards increased blocking, there are exceptions. The EC-Earth3 model predicts more blocking–like conditions northwest of the AP in summer and a pronounced ridge over the Bellingshausen Sea in winter, indicating a potential increase in blocking events. The INM-CM4 model projects a minor increase in summer Z500 heights off the western and southern AP, without clear blocking patterns over the AP, and negligible winter changes. Localized intensification is noted in the northern parts of the blocking domain and southern AP during extreme blocking conditions. These variations are mirrored in T2m anomalies, suggesting warming in the northern and southern sections of AP but little change elsewhere. The results of this study underscore the need to

* Corresponding author at: Departamento de Meteorología, Universidad de Valparaíso, Chile.
E-mail address: deniz.bozkurt@uv.cl (D. Bozkurt).

https://doi.org/10.1016/j.scitotenv.2024.172852
Received 29 December 2023; Received in revised form 13 April 2024; Accepted 26 April 2024
Available online 4 May 2024

more accurately capture complex blocking mechanisms and their impacts on regional climate patterns around the AP. We also suggest employing refined blocking definitions and incorporating a broader range of climate models to enhance our understanding of blocking patterns and their impacts in a changing climate.

1. Introduction

The Antarctic Peninsula (AP) has emerged as a key area of interest for climate change, extreme weather events, and their impacts. Recent observations indicate a high degree of year–to–year fluctuations, meaningful interdecadal variability, and strong long–term warming trends in near–surface air temperatures in the AP (Marshall, 2007; Jones et al., 2019; Turner et al., 2016; Oliva et al., 2017; Bozkurt et al., 2020; Carrasco et al., 2021). In addition to an overall warming trend, the AP faces an increased risk of extreme weather events. For instance, atmospheric rivers (ARs), which are long, narrow corridors of concentrated moisture in the atmosphere, are not only associated with intense precipitation but also with extremely high temperatures and melt events in the AP (Bozkurt et al., 2018; Xu et al., 2021; Wille et al., 2022; Clem et al., 2022; Zou et al., 2023; Gorodetskaya et al., 2023). Heatwaves and increased solar radiation during the austral summer season introduce a layer of complexity to the region's climate dynamics. Foehn winds over local topography can trigger extremely high temperatures and warm events, particularly on the leeward side of the AP (Elvidge et al., 2015; Bozkurt et al., 2018; Tri Datta et al., 2019; Elvidge et al., 2020; Turton et al., 2020; Laffin et al., 2022). These events and long–term warming have far–reaching implications for the cryosphere, including accelerated snow and glacier retreat, heightened ice shelf instability (Scambos et al., 2004; Rignot et al., 2019; González-Herrero et al., 2022; Wille et al., 2022; González-Herrero et al., 2024), and consequential impacts on both land and marine ecosystems (Convey and Smith, 2006; Siegert et al., 2019, 2023).

The AP is a complex climate zone where large–scale teleconnections and synoptic–scale weather patterns shape climate variability and the evolution of extreme weather events. The AP experiences the influence of the Southern Annular Mode (SAM) and the El Niño–Southern Oscillation (ENSO), both of which play a significant role in shaping regional circulation patterns (e.g., Marshall et al., 2006; Fogt et al., 2012; Clem et al., 2016; Yuan et al., 2018). The complex interplay between these important large–scale features, along with the influence of tropical sea surface temperature and convective variability, can create wave sources in the subtropics, exciting quasi–stationary wave trains that extend poleward and lead to major changes in regional circulation patterns around the AP (e.g., Fogt and Bromwich, 2006; Pezza et al., 2008; Clem et al., 2022). For instance, during El Niño and Madden–Julian oscillation events, Rossby wave trains emanating from the central Pacific Ocean can lead to anomalously high sea level pressure and increased blocking patterns across the southeast Pacific and the AP, thereby influencing the regional climate (Yuan and Martinson, 2001; Steig et al., 2012; Yuan et al., 2018; Henderson et al., 2018; Rondanelli et al., 2019).

Atmospheric blocking is broadly defined as an anomalous, quasi–-stationary anticyclonic circulation pattern that disrupts the propagation of cyclones and other weather systems (AMS, 2022). Understanding blocking patterns is crucial in the context of climate change, as these anomalous circulations can have far–reaching impacts on regional and global weather. The influence of blocking patterns is not limited to specific regions, as evidenced by their significant association with extreme weather events and climate variability across different parts of the world. For instance, studies have shown that blocking events can lead to prolonged periods of extreme temperatures, precipitation anomalies, and disruptions to typical atmospheric circulation patterns, affecting regions such as Europe, North America, and Greenland (e.g., Sousa et al., 2018; Brunner et al., 2018; Schaller et al., 2018; Barrett et al., 2020; Henderson et al., 2021; Wachowicz et al., 2021). In the Southern Hemisphere, blocking patterns can have significant societal consequences such as droughts and wildfires (Parker et al., 2014; Rodrigues and Woollings, 2017; Rodrigues et al., 2019). Similarly, the mid tropospheric trough-ridge couplet has been shown to trigger extreme meteorological events and AR landfalls across other parts of Antarctica (Wille et al., 2021; Pohl et al., 2021; Wille et al., 2024). Over the AP, Bozkurt et al. (2022) showed that blocking events were associated with warm episodes facilitated by northerly and northwesterly warm air transport, leading to significant increases in moisture transport and AR frequency. In addition, excessive summertime shortwave radiation during blocking can cause prolonged warm anomalies and lead to extensive melt events (Bevan et al., 2020; Banwell et al., 2021). The impact of blocking patterns on climate variability and extreme weather events underscores the need for a comprehensive understanding of their dynamics and potential changes in a warming climate.

General circulation models (GCMs) are essential tools for studying the response of the AP to a warming climate. These models can effectively simulate the complex interactions between large–scale atmospheric circulation patterns, regional climate systems, and the influence of external forcings, providing valuable projections of future climate scenarios. The Coupled Model Intercomparison Project (e.g., CMIP5 and CMIP6) model projections have recently provided valuable insights into potential changes in climate dynamics and extreme weather events, such as extreme high temperatures and melt events in the AP (Bozkurt et al., 2021; Gilbert and Kittel, 2021; Kittel et al., 2022; Zhu et al., 2023).

Additionally, modeling efforts can allow for the assessment of blocking patterns and uncertainties in extreme weather. Studies have highlighted major uncertainty regarding the frequency of blocking in different regions, mostly in the Northern Hemisphere. For instance, three generations of climate models have highlighted a persistent and consistent trend in underestimating blocking frequencies, with CMIP6 models facing challenges, especially in the winter European sector (Davini and D'Andrea, 2020). In a similar manner, using 10 Geophysical Fluid Dynamics Laboratory (GFDL) GCMs in the CMIP5 and CMIP6 repositories, Liu et al. (2022) stated that atmospheric blocking frequency faces a 50 % underestimation in the Atlantic–Europe region during December–February, a 60 % overestimation in the Pacific–North America region, and a 70 % overestimation in the southwest Pacific region during July–August.

Recent studies have also highlighted the significance of atmospheric blocking and its response to climate change. Projections indicate a consistent blocking frequency in the European–North Atlantic sector and Greenland and a shift towards reduced blocking and greater zonal flow conditions (de Vries et al., 2013; Woollings et al., 2018; Delhasse et al., 2021; Dorrington et al., 2022). In the Southern Hemisphere, blocking frequency is also projected to decrease, particularly in the Pacific during austral spring and summer, with a hint of meridional displacements (Parsons et al., 2016; Woollings et al., 2018).

The uncertainty in these projections underscores the challenges in modeling blocking events in a warming climate. They reinforce the need for further research and enhanced modeling techniques, particularly in the AP. In a recent study, Marín et al. (2022) analyzed atmospheric blocking around the AP from 1979 to 2018, noting increased blocking days over the AP in 1999–2018, especially during austral autumn, winter, and spring. A subsequent study by Bozkurt et al. (2022) emphasized the significant role of blocking conditions over the AP in triggering extreme temperatures and moisture transport. These studies notwithstanding, there remains a notable gap in the systematic evaluation and analysis of CMIP models' representation of blocking conditions over the AP. This gap hinders a comprehensive understanding of future climate scenarios in this region. Therefore, the current study primarily

aims to assess the performance of available CMIP6 models in simulating blocking conditions over the AP. Section 2 describes the data and methodology used in this study. Section 3 presents the results of evaluating CMIP6 models in representing blocking conditions over the AP for the historical period. It also includes projected changes in blocking patterns and temperature obtained from the top–ranking models. Section 4 summarizes and discusses the results.

2. Data and methodology

2.1. Dataset

This study relies on representations of the atmosphere in ERA5 and the CMIP6 models to explore blocking patterns over the AP. We analyzed the 500 hPa geopotential height (Z500) fields (downloaded for 1200 UTC with daily resolution) from the ERA5 reanalysis to calculate blocking indices. The ERA5 is a relatively new, state–of–the–art global reanalysis produced by the European Centre for Medium–Range Weather Forecasts (ECMWF) (Hersbach et al., 2020). It is based on an improved version of the Integrated Forecast System (IFS Cycle 41r2) and 4D–Var data assimilation, providing continually updated global gridded climatic data. ERA5 has a horizontal grid spacing of approximately 30 km and 137 vertical levels from the surface to a height of 80 km. We also analyzed six CMIP6 models (Eyring et al., 2016), including multi-member realizations from two models totaling ten simulations, focusing on Z500 and near–surface air temperature (T2m) as key variables. The selection of the GCMs was primarily driven by data availability constraints. Our CMIP6 analyses encompassed (1) historical experiments (1981–2010) with coupled uninitialized climate runs driven by historical greenhouse gas and aerosol forcings throughout the twentieth century, and (2) future climate projections (2071–2100) under the SSP5–8.5 climate change scenario, a high greenhouse gas emission scenario leading to substantial radiative forcing. More information about the CMIP6 models used in this study is found in Table 1.

2.2. Geographical setting

The geographical focus of the analysis covers the Drake Passage, northern and central AP, and Weddell and Bellingshausen Seas (90–30°W, 50–70°S, red polygon in Fig. 1) for the austral summer (December–January–February: DJF) and winter (June–July–August: JJA) seasons. The selected geographical area has displayed a propensity for persistent blocking ridges and anticyclonic conditions, particularly during recent summertime extreme weather events characterized by extreme high temperatures and ice melt (e.g., Bozkurt et al., 2018; Xu et al., 2021; Clem et al., 2022; Zou et al., 2023). This observation aligns with findings from Bozkurt et al. (2022), who highlighted the AP region as having a high potential to trigger extreme weather events.

Table 1
List of CMIP6 models used in this study to construct blocking indices over the Antarctic Peninsula.

Model name	Institution	Resolution in degrees (longitude x latitude)	Variant label	Abbreviation
CESM2-WACCM	NCAR, USA	1.25 × 0.94	r1i1p1f1	CESM2-W-R1
			r2i1p1f1	CESM2-W-R2
			r3i1p1f1	CESM2-W-R3
EC-Earth3	EC-Earth-Consortium, Europe	0.7 × 0.7	r1i1p1f1	EC-Earth3-R1
INM-CM4–8	INM, Russia	2.0 × 1.5	r1i1p1f1	INM-CM4-R1
INM-CM5–0				INM-CM5-R1
MRI-ESM2–0	MRI, Japan	1.13 × 1.13	r1i1p1f1	MRI-ESM2-R1
			r2i1p1f1	MRI-ESM2-R2
			r3i1p1f1	MRI-ESM2-R3
NorESM2-MM	NCC, Norway	1.25 × 0.94	r1i1p1f1	NorE-MM-R1

2.3. Methodology

Due to the varying spatial resolutions of the GCMs and ERA5 used in this study, all models and ERA5 underwent bilinear interpolation onto a common grid of 0.75°. We then calculated blocking indices by averaging Z500 mean values across our domain (red box in Fig. 1) for the historical and future periods. This approach resulted in daily time series of blocking, similar to the operational use of the Greenland Blocking Index (GBI, (Fang, 2004; Hanna et al., 2013, 2014)) by NOAA to assess blocking over Greenland. We then identified "very extreme blocking" for Z500 values surpassing the 95th (P95) percentile. The percentile threshold was computed separately for DJF and JJA seasons. The cumulative count of very extreme blocking days was derived by summing the days in each season surpassing the respective threshold.

To identify the two top–performing CMIP6 models, we ranked each based on their performance in capturing historical spatial patterns of Z500 fields and frequency distribution characteristics. The anomalies of T2m and Z500 during the P95 days from the ERA5 and the selected top–performing two models were then computed using a low-pass filter to smooth the daily variability. Anomalies on P95 days were calculated for each date as departures of 7–day mean values with respect to the seasonal mean climatology of historical and future periods. The statistical significance of T2m and Z500 anomalies in the ERA5 and the selected top–performing models was assessed using a bootstrap method at the 95 % confidence level. This involved conducting 2000 iterations with randomly selected daily composite anomalies (calculated with the 7–day running mean) and matching them with extreme blocking days (P95) by DJF and JJA seasons. For each grid point, an averaged T2m anomaly was considered significant at the 95 % confidence level if it fell outside the 2.5–97.5 percentile range of the bootstrap distribution. Non–significant anomalies were removed by masking grid points in figures to highlight the statistically significant points.

To refine our analysis of projected blocking patterns, we adopted the method outlined by Delhasse et al. (2021), which involves calculating the Z500 anomaly at each grid cell over the region of interest for the two top–performing models. This was achieved by subtracting the hemispheric mean Z500, averaged over the 50°S to 70°S latitudinal band for the period 1981–2010, from the Z500 at each grid cell for the corresponding periods. This approach helps to isolate the dynamic anomaly from broader hemispheric thermal influences, providing a clearer insight into the atmospheric blocking dynamics. In addition, blocking indices and temperature anomalies were calculated for the two top–performing models. For future scenarios (SSP5–8.5), a third–order polynomial was fitted to the area–weighted, season–averaged Z500 time series to account for potential acceleration in Z500 increase, following Dorrington et al. (2022) and Fabiano et al. (2021). The same anomaly calculation and significance test that were applied to the historical period were also applied to the future period.

3. Results

We begin our analysis by examining the historical years in CMIP6 models, focusing on blocking patterns over the AP throughout the entire analysis period as well as on extreme blocking days (P95). We next analyze projected changes in blocking, focusing on Z500 and T2m anomalies in the two top–performing models for the future period under the SSP5–8.5 scenario.

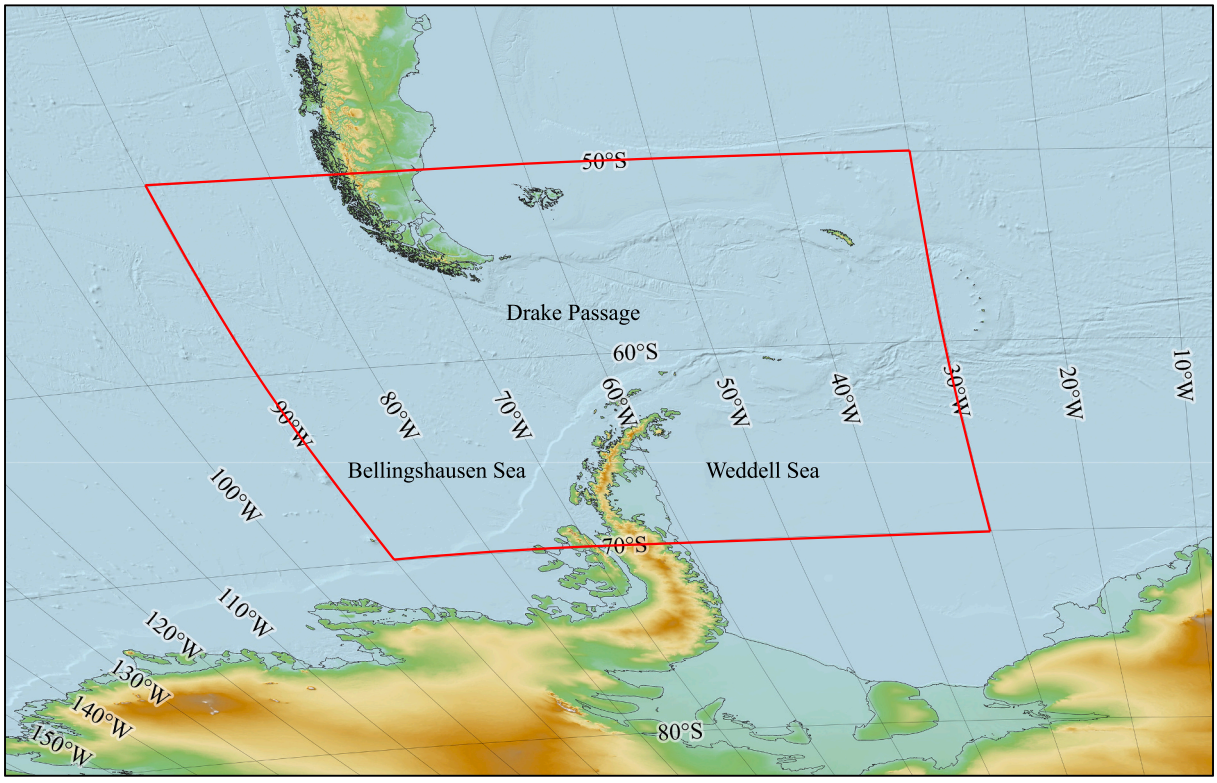

Fig. 1. Topographic map of the Antarctic Peninsula and its surrounding areas derived from ETOPO 2022. Red box corresponds to the region where blocking indices were determined.

3.1. *Historical period*

A comparison of historical Z500 heights in CMIP6 models with ERA5 reanalysis shows lower Z500 heights in the southern sections of the domain, with significant model disparities, particularly over the Drake Passage and South America. During DJF, some models indicate higher Z500 heights, with the INM-CM4-R1 closely aligning with ERA5 (Fig. S1). In the JJA season, these disparities widen, with a general shift towards more pronounced cyclonic activity, especially over the Drake Passage and Bellingshausen Sea (Fig. S2). EC-Earth3-R1 and INM-CM4-R1 show lesser variations, with EC-Earth3-R1 among the only model to show anticyclonic conditions in certain areas.

Figs. 2 and 3 depict the annual, DJF, and JJA distributions of Z500, averaged over the study domain, for ERA5 and each CMIP6 climate model. The figures present a comprehensive view of how well the CMIP6 climate models align with the ERA5 reanalysis over the blocking domain. Annually, all models show central peaks in Z500 heights shifted lower than the ERA5, suggesting an underestimation of the mean Z500

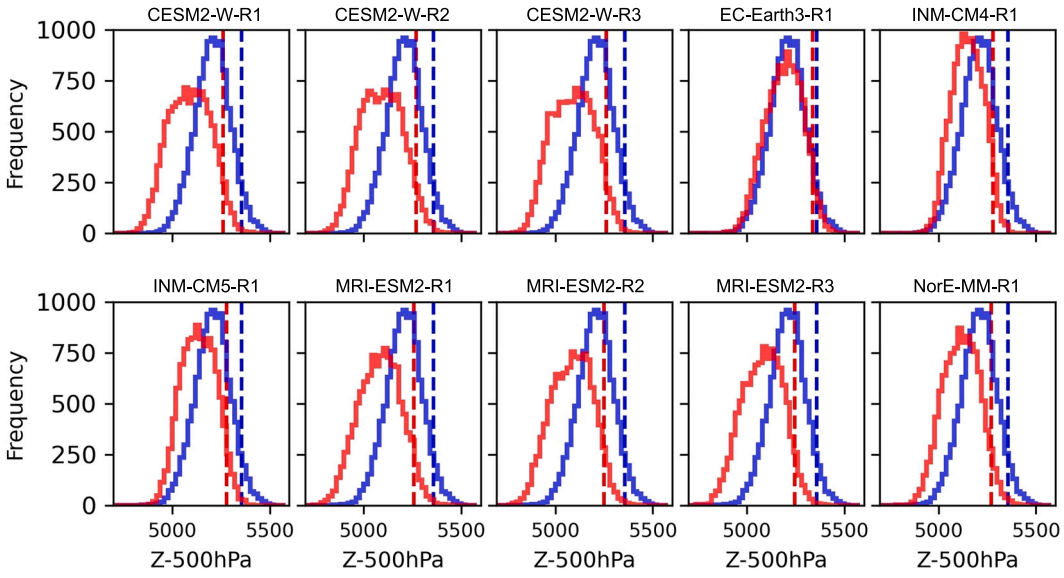

Fig. 2. Distribution of annual 500 hPa mean geopotential heights averaged over the blocking domain, as depicted in Fig. 1, for ERA5 (blue) and ten CMIP6 climate models (red). Vertical lines show the 95th percentile values for ERA5 (blue line) and CMIP6 models (red line).

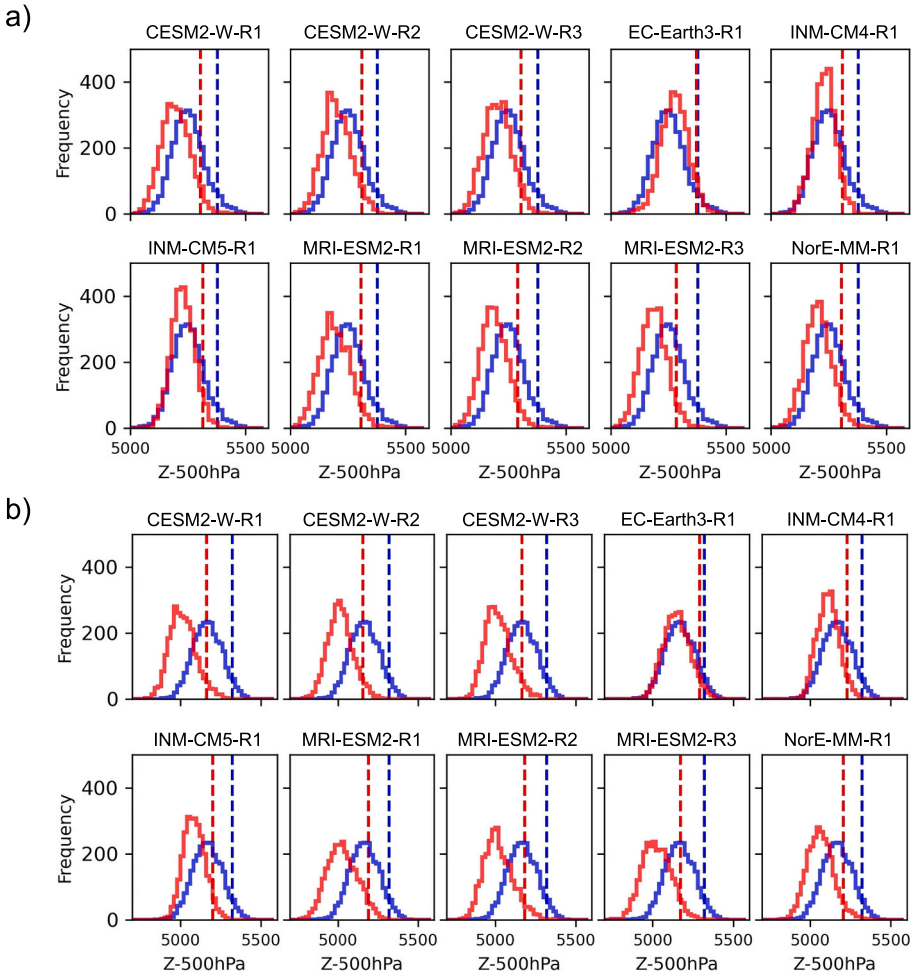

Fig. 3. As in Fig. 2, but for the a) DJF and b) JJA seasons.

heights (Fig. 2). Notably, EC-Earth3-R1 and INM-CM4-R1 display distributions more closely aligned with ERA5, with EC-Earth3-R1, in particular, showing a more reasonable match in both central tendency and variance. The overall underestimation persists in the DJF season (except for EC-Earth3-R1), with misaligned peaks and variance, failing to match the summer variability in ERA5 (Fig. 3a). The height differences in CMIP6 are more pronounced in the JJA season, with a significant shift indicating a notable underestimation of winter Z500 and an

Table 2
Evaluation metrics of annual and seasonal 500 hPa geopotential heights over the blocking domain.

	ERA5	CESM2-W-R1	CESM2-W-R2	CESM2-W-R3	EC-Earth3-R1	INM-CM4-R1	INM-CM5-R1	MRI-ESM2-R1	MRI-ESM2-R2	MRI-ESM2-R3	NorE-MM-R1
Annual											
Central difference	–	−116.50	−114.47	−116.54	−16.72	−57.62	−70.40	−123.03	−121.31	−125.49	−89.76
P95 difference	–	−93.87	−88.41	−93.91	−19.24	−77.67	−76.53	−99.73	−106.13	−112.08	−86.76
Standard dev.	91.53	106.59	107.67	107.88	94.45	80.40	88.60	107.54	105.08	103.66	94.24
Skewness	−0.06	0.01	0.06	0.00	−0.15	−0.04	0.01	−0.04	−0.08	−0.11	−0.01
DJF											
Central difference	–	−55.02	−51.18	−49.46	23.06	−23.49	−23.57	−59.82	−63.56	−66.47	−48.20
P95 difference	–	−72.51	−67.35	−72.05	−6.05	−69.12	−62.70	−72.37	−87.68	−94.80	−71.95
Standard dev.	70.67	62.66	62.75	60.82	59.05	49.62	50.76	66.96	59.67	57.95	60.01
Skewness	0.32	0.22	0.19	0.08	−0.03	−0.09	0.13	0.25	0.21	0.16	0.22
JJA											
Central difference	–	−152.54	−151.03	−148.77	−17.07	−55.68	−81.82	−139.38	−146.82	−143.36	−104.32
P95 difference	–	−158.60	−164.93	−153.96	−30.47	−92.29	−121.42	−130.38	−137.11	−148.24	−116.72
Standard dev.	90.70	82.54	79.19	81.79	82.33	66.89	66.64	93.95	89.82	89.28	82.04
Skewness	0.04	0.37	0.26	0.44	0.18	0.14	0.19	0.18	0.48	0.20	0.36

inaccurate representation of the seasonal variability (Fig. 3b). In contrast to the biases observed for other CMIP6 models, EC-Earth3-R1 and INM-CM4-R1 are more aligned with ERA5 across DJF and JJA. Notably, EC-Earth3-R1 exhibits a distribution that is particularly close to ERA5 during the JJA season, with a central peak and variance that closely reflect the Z500 distribution in ERA5. INM-CM4-R1, while still aligned well with ERA5, demonstrates slightly less of a match with ERA5 than EC-Earth3-R1, especially in terms of capturing the central tendency and spread of winter Z500 heights.

Table 2 presents annual and seasonal Z500 heights over the blocking domain, comparing CMIP6 climate models against the ERA5 for the period 1981–2010. For the annual period, EC-Earth3-R1 shows the smallest central and P95 differences, suggesting it has the closest agreement with ERA5 of any CMIP6 model we analyzed. INM-CM4-R1 also shows a relatively low central difference and standard deviation, indicating its variability is more in line with ERA5 compared to other models. Across the board, models have higher standard deviations than ERA5, implying more variability in the model outputs. Skewness values are mostly similar to ERA5, pointing to a comparable distribution asymmetry in the models. In the DJF season, both EC-Earth3-R1 and INM-CM4-R1 display notably smaller central differences compared to ERA5, suggesting a more reasonable alignment with the reanalysis data. Other models present larger central and P95 differences, indicating greater deviation from ERA5. EC-Earth3-R1 and INM-CM4-R1 exhibit the lowest annual standard deviations among the models, signifying that their interannual variability is most similar to ERA5's. Skewness across most models is positive, reflecting a tendency towards higher Z500, similar to ERA5. In the JJA season, EC-Earth3-R1 stands out with significantly lower central and P95 differences compared to ERA5, suggesting a better representation of winter variations of Z500. INM-CM4-R1 also shows lower central differences in Z500, although not as pronounced as EC-Earth3-R1, indicating a better alignment with ERA5 than the other CMIP6 models. The standard deviations for these models in JJA are similar to the annual metrics. Skewness varies, with EC-Earth3-R1 and INM-CM4-R1 displaying less skew towards higher Z500 values, indicating a distribution that more closely resembles ERA5 than the other models.

The results so far reveal that EC-Earth3-R1 and INM-CM4-R1 agree best with Z500 heights in the ERA5. Therefore, to assess the relationships between Z500 and T2m anomalies during P95 days, our analysis will focus on these two models. Fig. 4 shows DJF and JJA mean Z500 anomalies during P95 days from ERA5, EC-Earth3-R1, and INM-CM4-R1. The ERA5 reanalysis shows significant positive Z500 anomalies in the DJF season, with the core of the anomaly located over the northern part of the AP (Fig. 4a). In the JJA season, the significant anomalies become more intense and widespread, indicative of stronger blocking activity during the austral winter (Fig. 4b). EC-Earth3-R1 and INM-CM4-R1 capture the significant positive Z500 anomaly pattern seen in ERA5, yet some differences are evident. During the DJF season, Z500 anomalies from EC-Earth3-R1, while extensive, are less intense than those observed in ERA5, indicating a broader but weaker signal for blocking activity (Fig. 4c). In JJA, EC-Earth3-R1 shows a marked increase in the intensity of the Z500 anomalies, consistent with stronger winter blocking, but the pattern of positive Z500 anomalies is displaced to the north of the AP, unlike that shown by ERA5 (Fig. 4d). INM-CM4-R1 captures the spatial pattern of the Z500 anomalies better than EC-Earth3-R1 in the DJF season, yet the anomalies are less intense (Fig. 4e). In addition, while still capturing the broad pattern in JJA, INM-CM4-R1 presents a less intense anomaly, especially in the core region, compared to both EC-Earth3-R1 and ERA5 (Fig. 4f).

Fig. 5 shows mean DJF and JJA T2m anomalies during P95 days from ERA5, EC-Earth3-R1, and INM-CM4-R1. The ERA5 reanalysis shows

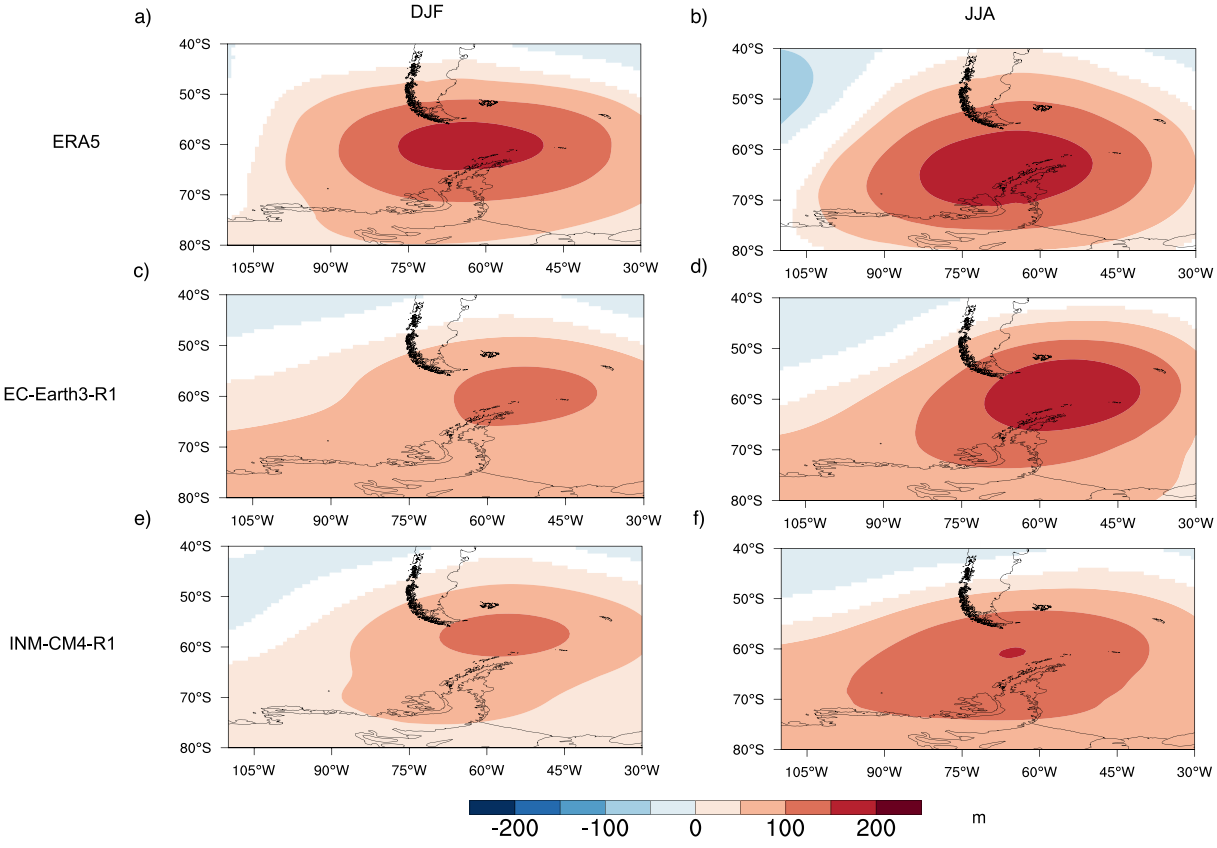

Fig. 4. Composite mean a) DJF and b) JJA 500 hPa geopotential height anomalies (1981–2010, shaded) for P95 days over the region of interest obtained from ERA5. c) and d) are the same as in a) and b) but for EC-Earth3-R1, respectively. e) and f) are the same as in a) and b) but for INM-CM4-R1, respectively. Grid points are masked in white if the anomalies are not statistically significant at the 95 % confidence level (determined through a 2000-trial bootstrap resampling method).

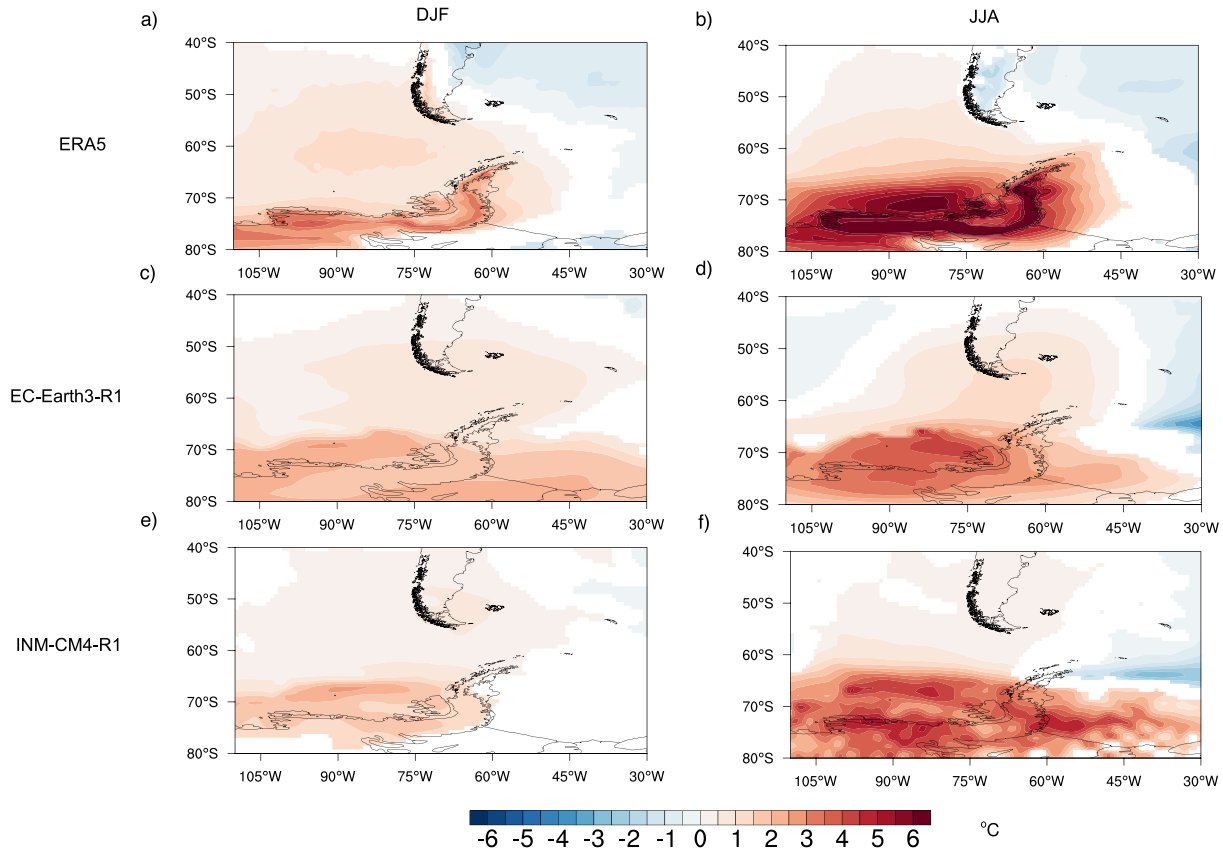

Fig. 5. As in Fig. 4 but for near-surface temperature anomalies.

moderate significant warming anomalies over the AP in the DJF season, while in the JJA season, it exhibits a more intense significant warming pattern extending over the Peninsula, particularly over the coastal areas of the Bellingshausen Sea and the surrounding oceanic regions as well as the leeward side of the AP ($> +6$ °C) (Figs. 5a, b). Both EC-Earth3-R1 and INM-CM4-R1 generally replicate the significant warming observed in ERA5 during P95 blocking. In the DJF season, EC-Earth3-R1 exhibits a warming pattern that is less intense compared to ERA5, albeit covering a more widespread area (Fig. 5c). In the JJA season, EC-Earth3-R1 presents a notable increase in warming intensity, indicating the surface response to more intense winter blocking events. Yet, it still falls short of the warming magnitudes shown in ERA5 (Fig. 5d). INM-CM4-R1 also shows less warming than ERA5 in the DJF season, but with a similar distribution to ERA5 that is not as extensive as that shown in EC-Earth3-R1 (Fig. 5e). In the JJA season, INM-CM4-R1 demonstrates a slight uptick in warming intensity compared to EC-Earth3-R1, aligning more closely with the more intense warming anomalies seen in ERA5. Finally, the INM-CM4-R1 shows a spread–out warming pattern in the southern parts of the domain and insignificant changes over the northern AP (Fig. 5f).

In summary, both EC-Earth3-R1 and INM-CM4-R1 capture the general patterns of ERA5 Z500 height and T2m temperature anomalies during P95 days, reflecting the overall observed spatial distribution and seasonal amplification. While INM-CM4-R1 slightly better represents the core of Z500 anomalies in DJF and the intensified near–surface warming in JJA, EC-Earth3-R1 displays broader anomaly patterns across both seasons. Despite these differences, both models exhibit less severe anomalies compared to ERA5, yet they still express the fundamental characteristics of blocking events in the region.

3.2. Future period

Fig. 6 shows mean Z500 height anomalies in each grid cell over the periods 1981–2010 and 2071–2100 (anomalies with respect to the 1981–2010 mean hemispheric Z500 height averaged over 50° and 70°S) for EC-Earth3-R1 and INM-CM4-R1 models. For the DJF season, the EC-Earth3-R1 model projects an increase in height off the northwest AP (Figs. 6a-b), which indicates a higher tendency for blocking events in this region. The INM-CM4-R1 model shows increased Z500 anomalies off the western and southern AP but does not exhibit an increase in blocking over the AP, instead showing a modest change in Z500 with respect to the historical period (Figs. 6c-d). In the JJA season, the EC-Earth3-R1 model's future projections exhibit a pronounced ridge formation with increased positive Z500 anomalies over the Bellingshausen Sea, pointing to an increased tendency for blocking conditions, but a stable or decreased tendency over the AP and the Weddell Sea (Figs. 6e-f). The INM-CM4-R1 model does not show a significant overall increase in positive anomalies for the JJA season, however, there is a slight increase over the northern parts of the AP, associated with a ridge extending from southern South America to the Atlantic sector (Figs. 6g-h).

Fig. 7 shows projected DJF and JJA Z500 anomalies during P95 days from EC-Earth3-R1 and INM-CM4-R1 for the period 2071–2100. In DJF, EC-Earth3-R1 indicates a slight but significant increase in Z500 anomalies off the northwestern parts of the AP compared to the historical period (Fig. 7a). In JJA, EC-Earth3-R1 shows no significant change in Z500 anomalies compared to those in the historical period, indicating no change in the intensity of future P95 blocking, except for some parts of the northwestern blocking domain (Fig. 7b). Compared to EC-Earth3-R1, the INM-CM4-R1 model reveals widespread and significant increases in DJF Z500 over the southernmost areas of the AP. However, it does not indicate any significant rise in Z500 over the Drake Passage and

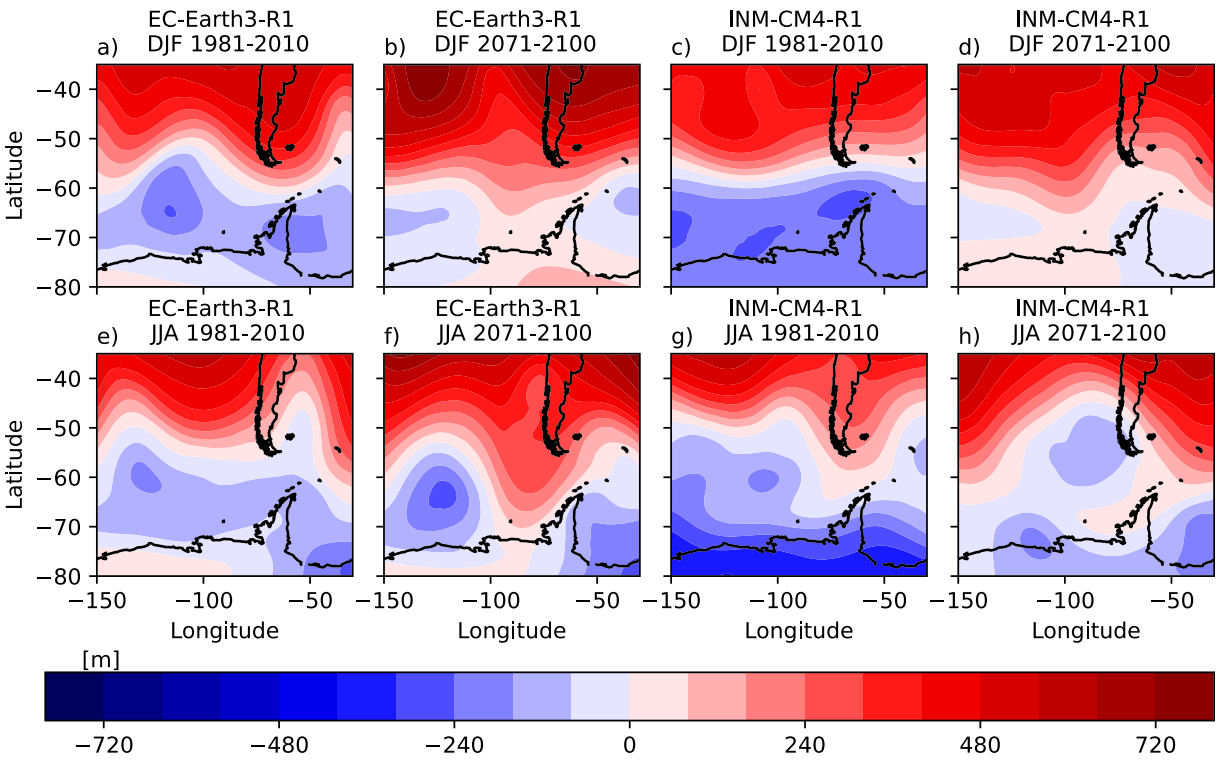

Fig. 6. Mean DJF 500 hPa geopotential height anomalies in each grid cell with respect to the 1981–2010 mean hemispheric 500 hPa geopotential height values averaged over 50° and 70°S for a) EC-Earth3-R1 (1981–2010), b) EC-Earth3-R1 (2071–2100), c) INM-CM4-R1 (1981–2010) and d) INM-CM4-R1 (2071–2100). e), f), g) and h) are the same as in a), b), c) and d) but for JJA season, respectively.

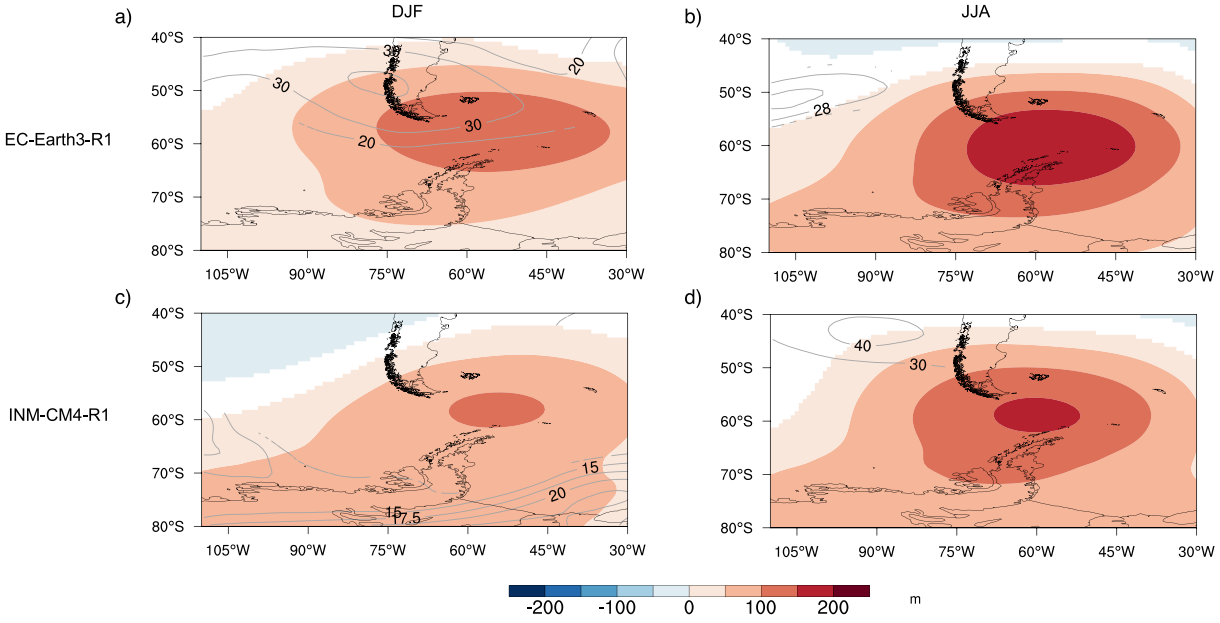

Fig. 7. Composite mean 500 hPa geopotential height anomalies (shaded) for P95 days over the region of interest obtained from EC-Earth3-R1 for a) DJF and b) JJA seasons for the period 2071–2100 under the SSP5–8.5 scenario. c) and d) are the same as in a) and b) but for INM-CM4-R1, respectively. Grid points are masked in white if the anomalies are not statistically significant at the 95 % confidence level (determined through a 2000–trial bootstrap resampling method). The gray contour lines represent the significant positive differences between future and historical 500 hPa geopotential height anomalies during blocking days.

the northern parts of the AP during future P95 days (Fig. 7c). For JJA, INM-CM4-R1 primarily exhibits no significant increases in Z500, similar to EC-Earth3-R1, with the exception of some significant height increases noted in the northwestern sector of the domain (Fig. 7d).

The T2m anomalies during future P95 show an overall pattern consistent with the Z500 anomalies (Fig. 8). For EC-Earth3-R1, DJF P95 blocking conditions in the future are not associated with a significant rise in T2m anomalies, with the exception of a slight warming (around + 0.5 °C) over the northernmost AP and the northern sections of the blocking domain (Fig. 8a). This localized T2m increase aligns with the

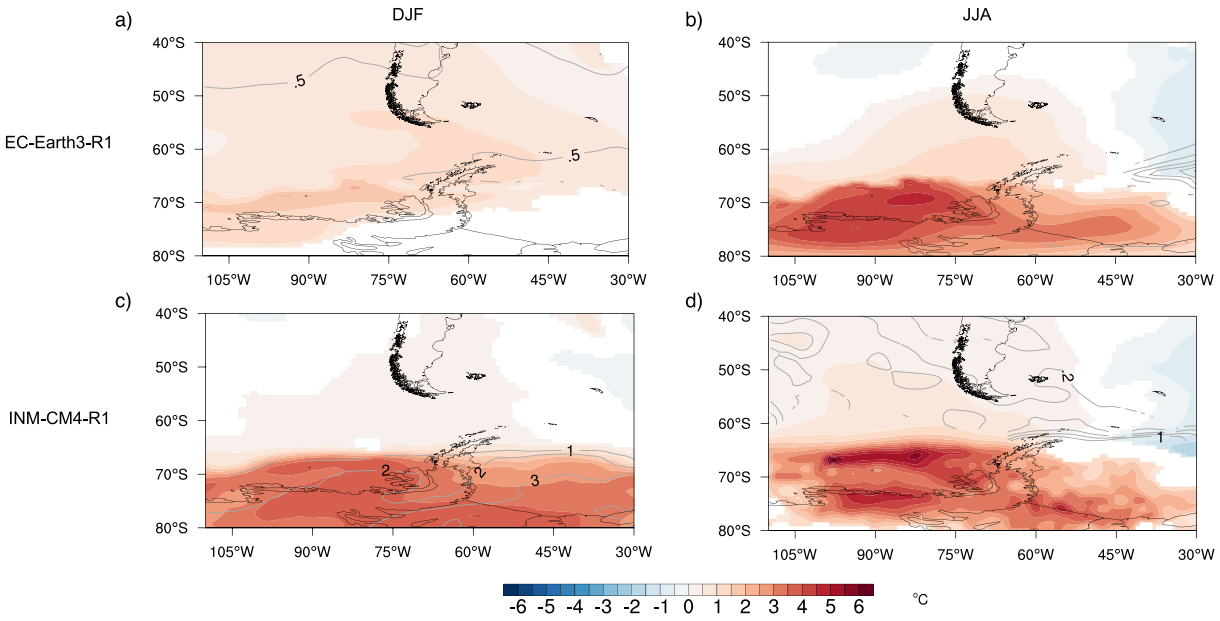

Fig. 8. As in Fig. 7 but for near–surface temperature anomalies.

previously noted positive Z500 anomalies. During the JJA season, EC-Earth3-R1 shows little to no change in T2m anomalies over the blocking domain (Fig. 8b), which parallels the lack of significant change in Z500 anomalies seen for this season (see Fig. 7b). This consistency indicates that the T2m response during extreme (P95) blocking may remain relatively stable compared to the historical period.

The INM-CM4-R1 model in DJF projects a more notable increase in T2m anomalies during extreme (P95) blocking, particularly over the central and southern parts of the AP, with temperature anomalies ranging between + 1 to + 3 °C over the historical period (Fig. 8c). This pronounced warming aligns with the significant Z500 increases indicated in the same regions in Fig. 7c, suggesting a strong correlation between Z500 and T2m during P95 days. In JJA, similar to EC-Earth3-R1, the INM-CM4-R1 model shows minimal to no change in T2m anomalies, suggesting that P95 conditions may not result in significant T2m anomalies during winter (Fig. 8d). The only exceptions are slight but significant T2m increases over the northernmost AP and northern regions of the blocking domain, which correspond with increased Z500 anomalies under future P95.

4. Summary and discussion

This study evaluates historical (1981–2010) and future (2071–2100, SSP5–8.5) blocking patterns over the Antarctic Peninsula (AP) on annual, austral summer (December–January–February, DJF), and winter (June–July–August, JJA) timescales using ERA5 reanalysis and six CMIP6 models, including multi-member realizations from two models totaling ten simulations. The analysis is based on 500-hPa geopotential height (Z500) and near-surface air temperature (T2m) anomalies. Climatological analysis reveals significant discrepancies between CMIP6 and ERA5 reanalysis in capturing the historical Z500 and blocking patterns and associated T2m anomalies. We also analyzed future projections, utilizing the two top-ranking CMIP6 models (EC-Earth3-R1 and INM-CM4-R1) based on their historical performance.

In the future period, the EC-Earth3-R1 model predicts blocking-like conditions to the northwest of the AP during the summer and a significant ridge pattern over the Bellingshausen Sea in the winter, hinting at potential blocking events there, too. Meanwhile, the INM-CM4-R1 model predicts an increase in Z500 heights off the western and southern Peninsula in summer, (although this height rise itself does not necessarily indicate blocking over the AP), and the model projects minimal changes in blocking in the winter season. The variations in the models highlight different dynamic responses to future climate. Following this signal, for the period of 2071–2100, there is generally no significant change in Z500 anomalies during P95 blocking over the northern AP and Drake Passage, except for localized intensification in the northern parts of the blocking domain and southern AP. The future T2m anomalies during P95 blocking are mostly consistent with Z500 anomalies, featuring localized warming in the northernmost and southern regions of the AP with negligible temperature anomalies in other areas.

The findings suggest that while some models demonstrate relatively better performance in capturing historical blocking patterns, there remain significant discrepancies in the representation of interannual variability (not shown) and the overall spatial distribution of blocking events, particularly in JJA. These discrepancies underscore the complexities involved in accurately representing historical blocking patterns and associated T2m anomalies in the AP region. Building on the insights from the historical period, the future projections analyzed in this study highlight notable differences in T2m response to DJF blocking events in models EC-Earth3-R1 and INM-CM4-R1. These differences may be attributable to a range of potential factors that govern T2m responses to blocking.

While there is a lack of specific studies focusing on atmospheric blocking over the AP, the existing literature provides insights into the potential uncertainties in these models, uncertainties which can also affect future blocking projections and their impacts. These uncertainties may be attributed to model errors arising from large–scale circulation biases, tropical–polar teleconnections, atmosphere–ocean interactions, internal variability, and local factors such as topography and sea–ice distribution (e.g., Woods et al., 2013; Masato et al., 2014; Lee and Ahn, 2016; Woollings et al., 2018). For instance, Bracegirdle et al. (2020) highlights that although the CMIP6 models better represent Southern Hemisphere westerlies with reduced equatorward bias and improved timescales (when compared to CMIP5 models), they still struggle to reproduce the Amundsen Sea Low. The Amundsen Sea Low is a key feature in the Southern Hemisphere atmospheric circulation and plays a significant role in shaping the regional climate, including the occurrence of blocking. The expansion of the Hadley cell in CMIP6 models, particularly over the Pacific sector, has also been shown to affect blocking due to a greater sensitivity to the Hadley cell circulation (Grise and Davis, 2020). The expansion of the Hadley circulation can impact blocking

patterns by altering the latitudinal position of the subtropical jet streams. This expansion may also modify large–scale atmospheric flow patterns, influencing blocking event frequency and persistence. In addition, the under-representation of tropical–polar teleconnections within CMIP models (e.g., Yuan et al., 2018) can introduce uncertainties in blocking patterns. These errors may disrupt the modeled large–scale atmospheric circulation, impacting the frequency and characteristics of blocking events worldwide, including over the AP. It is also important to note that the differences in the representation of historical blocking patterns among the models may be influenced by the models' (in)ability to capture the dynamics of interannual and interdecadal variability. The CMIP6 models may struggle to effectively capture these complex, fluctuating patterns over both annual and decadal scales (e.g., Fogt and Bromwich, 2006; Meehl et al., 2016; Clem et al., 2016; Turner et al., 2016; Fogt and Marshall, 2020).

In addition to large–scale circulations, local–scale factors can introduce uncertainties in climate models, affecting their ability to accurately represent and project blocking conditions and their associated impacts. For instance, Casagrande et al. (2023) noted that despite advancements in the sea ice representation, CMIP6 models are still unable to accurately represent the regional sea ice. Sea ice conditions can significantly affect the surface impacts of blocking, particularly the T2m anomalies, by modifying the surface energy balance and the local circulations during blocking conditions. These changes can also influence the duration and intensity of blocking events, impacting downstream temperatures. In this respect, the differences in T2m response to DJF blocking between EC-Earth3-R1 and INM-CM4-R1 in future projections may be partially attributed to how these models represent sea-ice conditions. Given that models may still struggle with regional sea-ice representation, this could lead to a divergence in how T2m responds to blocking conditions, especially over the AP, which is often bordered by sea ice. The potential limitations from coarse resolution in CMIP6 models may also result in challenges when capturing T2m responses to blocking patterns. The complex topography of the AP, combined with insufficient model resolution, can hinder the representation of blocking–triggered foehn conditions and warming amplification, particularly on the leeward side of the AP (Bozkurt et al., 2022).

The impacts of blocking conditions over the AP extend beyond atmospheric circulation changes, significantly influencing regional climate extremes, notably heatwaves. Given the projected increase in heatwave occurrences in the AP (Feron et al., 2021), it is imperative to conduct more detailed studies to delve deeper into the connection between blocking events and heatwaves, as well as their future variability. The connection between blocking and heatwave events is particularly critical, as such patterns can induce prolonged periods of anomalously high temperatures through changes in atmospheric circulation and increased solar radiation (Bevan et al., 2020; Banwell et al., 2021). Furthermore, these blocking events are integral in influencing AR activities, which are significant for transporting moisture and heat and contributing to precipitation and temperature extremes in Antarctica (Pohl et al., 2021; Turner et al., 2021; Wille et al., 2022; Baiman et al., 2023; Lu et al., 2023; Maclennan et al., 2023; Wille et al., 2024). The combined impact of blocking on T2m anomalies and ARs can intensify melt events, affecting ice shelf stability and glacial dynamics (Wille et al., 2021; Xu et al., 2021; Clem et al., 2022; Zou et al., 2023; Gorodetskaya et al., 2023). This interconnectedness underscores the importance of understanding how blocking events critically impact the AP's ice shelves and glaciers, influencing sea-level rise and affecting marine and terrestrial ecosystems, thereby emphasizing the need for integrated climate models to predict and mitigate their broad environmental consequences.

Future research should further investigate how anthropogenic climate change modulates the impacts of blocking patterns on the cryosphere, energy balance, and regional climate in the AP. These investigations should assess projected changes in moisture transport associated with blocking events and their implications for temperature and sea-ice patterns as well as melt events. Understanding the interplay between atmospheric blocking and moisture transport and how they jointly affect the surface energy balance and regional climate is crucial. These future studies will enhance our comprehension of the projected impacts of blocking patterns on moisture transport, melt events, and surface energy balance in the AP region, offering valuable insights for climate projections. Finally, this study's approach, centered on area-averaged blocking, might prevent a deeper investigation into blocking mechanisms and their projected impacts. Adopting different blocking definitions and incorporating an even more diverse range of climate models could significantly advance our understanding of blocking patterns and their impacts in the context of climate change.

CRediT authorship contribution statement

Deniz Bozkurt: Writing – review & editing, Writing – original draft, Visualization, Validation, Supervision, Methodology, Investigation, Formal analysis, Data curation, Conceptualization. **Julio C. Marín:** Writing – review & editing, Visualization, Validation, Methodology, Investigation, Formal analysis, Data curation, Conceptualization. **Cristina Verdugo:** Investigation, Data curation. **Bradford S. Barrett:** Writing – review & editing, Conceptualization.

Declaration of competing interest

The authors declare that they have no known competing financial interests or personal relationships that could have appeared to influence the work reported in this paper.

Data availability

ERA5 reanalysis data are available on the Copernicus Climate Change Service (C3S) Climate Data Store: https://cds.climate.copernicus.eu/. The CMIP6 data utilized in this study were obtained from the Earth System Grid Federation (ESGF). We accessed the data through their portal, available at https://esgf-node.llnl.gov/search/cmip6/. Blocking datasets are available upon request.

Acknowledgements

DB and JCM acknowledge support from the Centro de Estudios Atmosféricos y Cambio Climático (CEACC), Universidad de Valparaíso. DB acknowledges support from ANID–FONDECYT–1240190, ANID–FONDAP–1523A0002 and COPAS COASTAL ANID FB210021. We also acknowledge the World Climate Research Programme's Working Group on Coupled Modeling, which coordinated and promoted CMIP6. We further thank the climate modeling institutions for producing and making available their model output. We are grateful to Sergi González-Herrero for his constructive and helpful comments, which greatly improved the quality of the manuscript.

Appendix A. Supplementary data

Supplementary data to this article can be found online at https://doi.org/10.1016/j.scitotenv.2024.172852.

References

AMS, 2022. Blocking. American Meteorological Society, Available online at. https://glossary.ametsoc.org/wiki/Blocking.

Baiman, R., Winters, A.C., Lenaerts, J., Shields, C.A., 2023. Synoptic drivers of atmospheric river induced precipitation near Dronning Maud Land, Antarctica. J. Geophys. Res. Atmos. 128, e2022JD037859 https://doi.org/10.1029/2022JD037859.

Banwell, A.F., Datta, R.T., Dell, R.L., Moussavi, M., Brucker, L., Picard, G., Shuman, C.A., Stevens, L.A., 2021. The 32-year record-high surface melt in 2019/2020 on the northern George VI Ice Shelf, Antarctic Peninsula. Cryosphere 15, 909–925. https://doi.org/10.5194/tc-15-909-2021.

Barrett, B.S., Henderson, G.R., McDonnell, E., Henry, M., Mote, T., 2020. Extreme Greenland blocking and high-latitude moisture transport. Atmos. Sci. Lett. 21, e1002.
Bevan, S., Luckman, A., Hendon, H., Wang, G., 2020. The 2020 Larsen C Ice Shelf surface melt is a 40-year record high. Cryosphere 14, 3551–3564. https://doi.org/10.5194/tc-14-3551-2020.
Bozkurt, D., Rondanelli, R., Marín, J., Garreaud, R., 2018. Foehn event triggered by an atmospheric river underlies record-setting temperature along continental Antarctica. J. Geophys. Res. Atmos. 123, 3871–3892. https://doi.org/10.1002/2017JD027796.
Bozkurt, D., Bromwich, D.H., Carrasco, J., Hines, K.M., Maureira, J.C., Rondanelli, R., 2020. Recent near-surface temperature trends in the Antarctic Peninsula from observed, reanalysis and regional climate model data. Adv. Atmos. Sci. 37, 477–493. https://doi.org/10.1007/s00376-020-9183-x.
Bozkurt, D., Bromwich, D.H., Carrasco, J., Rondanelli, R., 2021. Temperature and precipitation projections for the Antarctic Peninsula over the next two decades: contrasting global and regional climate model simulations. Clim. Dyn. 56, 3853–3874. https://doi.org/10.1007/s00382-021-05667-2.
Bozkurt, D., Marín, J.C., Barrett, B.S., 2022. Temperature and moisture transport during atmospheric blocking patterns around the Antarctic Peninsula. Weath. Clim. Extrem. 38, 100506 https://doi.org/10.1016/j.wace.2022.100506.
Bracegirdle, T.J., Holmes, C.R., Hosking, J.S., Marshall, G.J., Osman, M., Patterson, M., Rackow, T., 2020. Improvements in circumpolar Southern Hemisphere extratropical atmospheric circulation in CMIP6 compared to CMIP5. Earth and Space. Science 7, e2019EA001065. https://doi.org/10.1029/2019EA001065.
Brunner, L., Schaller, N., Anstey, J., Sillmann, J., Steiner, A.K., 2018. Dependence of present and future European temperature extremes on the location of atmospheric blocking. Geophys. Res. Lett. 45, 6311–6320. https://doi.org/10.1029/2018GL077837.
Carrasco, J.F., Bozkurt, D., Cordero, R.R., 2021. A review of the observed air temperature in the Antarctic Peninsula. Did the warming trend come back after the early 21st hiatus? Pol. Sci. 100653 https://doi.org/10.1016/j.polar.2021.100653.
Casagrande, F., Stachelski, L., de Souza, R.B., 2023. Assessment of Antarctic Sea ice area and concentration in coupled model Intercomparison project phase 5 and phase 6 models. Int. J. Clim. 43, 1314–1332. https://doi.org/10.1002/joc.7916.
Clem, K.R., Renwick, J.A., McGregor, J., Fogt, R.L., 2016. The relative influence of ENSO and SAM on Antarctic peninsula climate. J. Geophys. Res. Atmos. 121, 9324–9341. https://doi.org/10.1002/2016JD025305.
Clem, K.R., Bozkurt, D., Kennett, D., King, J.C., Turner, J., 2022. Central tropical Pacific convection drives extreme high temperatures and surface melt on the Larsen C Ice Shelf. Antarctic Peninsula. Nat. Commun. 13, 3906. https://doi.org/10.1038/s41467-022-31119-4.
Convey, P., Smith, R.I.L., 2006. Responses of terrestrial Antarctic ecosystems to climate change. Plant Ecol. 182, 1–10.
Davini, P., D'Andrea, F., 2020. From CMIP3 to CMIP6: Northern Hemisphere atmospheric blocking simulation in present and future climate. J. Clim. 33, 10021–10038. https://doi.org/10.1175/JCLI-D-19-0862.1.
de Vries, H., Woollings, T., Anstey, J., Haarsma, R.J., Hazeleger, W., 2013. Atmospheric blocking and its relation to jet changes in a future climate. Clim. Dyn. 41, 2643–2654. https://doi.org/10.1007/s00382-013-1699-7.
Delhasse, A., Hanna, E., Kittel, C., Fettweis, X., 2021. Brief communication: CMIP6 does not suggest any atmospheric blocking increase in summer over Greenland by 2100. Int. J. Climatol. 41, 2589–2596. https://doi.org/10.1002/joc.6977.
Dorrington, J., Strommen, K., Fabiano, F., Molteni, F., 2022. Cmip6 models trend toward less persistent European blocking regimes in a warming climate. Geophys. Res. Lett. 49 https://doi.org/10.1029/2022GL100811.
Elvidge, A.D., Renfrew, I.A., King, J.C., Orr, A., Lachlan-Cope, T.A., Weeks, M., Gray, S. L., 2015. Foehn jets over the Larsen C Ice Shelf, Antarctica. Q. J. R. Meteorol. Soc. 141, 698–713. https://doi.org/10.1002/qj.2382.
Elvidge, A.D., Kuipers-Munneke, P., King, J.C., Renfrew, I.A., Gilbert, E., 2020. Atmospheric drivers of melt on Larsen C ice shelf: surface energy budget regimes and the impact of Foehn. J. Geophys. Res. Atmos. 125, e2020JD032463 https://doi.org/10.1029/2020JD032463.
Eyring, V., Bony, S., Meehl, G.A., Senior, C.A., Stevens, B., Stouffer, R.J., Taylor, K.E., 2016. Overview of the Coupled Model Intercomparison Project Phase 6 (CMIP6) experimental design and organization. Geosci. Model Dev. 9, 1937–1958. https://doi.org/10.5194/gmd-9-1937-2016.
Fabiano, F., Meccia, V.L., Davini, P., Ghinassi, P., Corti, S., 2021. A regime view of future atmospheric circulation changes in northern mid-latitudes. Weather Clim. Dynam. 2, 163–180. https://doi.org/10.5194/wcd-2-163-2021.
Fang, Z., 2004. Statistical relationship between the Northern Hemisphere sea ice and atmospheric circulation during wintertime. In: Observation. Theory and Modeling of Atmospheric Variability, Selected Papers of Nanjing Institute of Meteorology Alumni in Commemoration of Professor Jijia Zhang. World Scientific, pp. 131–141.
Feron, S., Cordero, R.R., Damiani, A., Malhotra, A., Seckmeyer, G., Llanillo, P., 2021. Warming events projected to become more frequent and last longer across Antarctica. Sci. Rep. 19564 https://doi.org/10.1038/s41598-021-98619-z.
Fogt, R.L., Bromwich, D.H., 2006. Decadal variability of the ENSO teleconnection to the high-latitude south pacific governed by coupling with the southern annular mode. J. Clim. 19, 979–997.
Fogt, R.L., Marshall, G.J., 2020. The southern annular mode: variability, trends, and climate impacts across the southern hemisphere. WIREs Climate Change 11. https://doi.org/10.1002/wcc.652.
Fogt, R.L., Jones, J.M., Renwick, J., 2012. Seasonal zonal asymmetries in the southern annular mode and their impact on regional temperature anomalies. J. Clim. 25, 6253–6270. https://doi.org/10.1175/JCLI-D-11-00474.1.
Gilbert, E., Kittel, C., 2021. Surface melt and runoff on Antarctic ice shelves at 1.5°c, 2°c, and 4°c of future warming. Geophys. Res. Lett. 48 https://doi.org/10.1029/2020GL091733.
González-Herrero, S., Barriopedro, D., Trigo, R.M., López-Bustins, J.A., Oliva, M., 2022. Climate warming amplified the 2020 record-breaking heatwave in the Antarctic Peninsula. Commun. Earth Environ. 3, 122. https://doi.org/10.1038/s43247-022-00450-5.
González-Herrero, S., Navarro, F., Pertierra, L.R., Oliva, M., Dadic, R., Peck, L., Lehning, M., 2024. Southward mitigation of the zero-degree isotherm latitude over the Southern Ocean and Antarctic peninsula. Sci. Total Environ. 912, 168473 https://doi.org/10.1016/j.scitotenv.2023.168473.
Gorodetskaya, I.V., Durán-Alarcón, C., González-Herrero, S., et al., 2023. Record-high Antarctic Peninsula temperatures and surface melt in February 2022: a compound event with an intense atmospheric river. NPJ Clim. Atmos. Sci. 6, 202. https://doi.org/10.1038/s41612-023-00529-6.
Grise, K.M., Davis, S.M., 2020. Hadley cell expansion in CMIP6 models. Atmos. Chem. Phys. 20, 5249–5268. https://doi.org/10.5194/acp-20-5249-2020.
Hanna, E., Jones, J.M., Cappelen, J., Mernild, S.H., Wood, L., Steffen, K., Huybrechts, P., 2013. The influence of North Atlantic atmospheric and oceanic forcing effects on 1900-2010 Greenland summer climate and ice melt/runoff. Int. J. Climatol. 33, 862–880. https://doi.org/10.1002/joc.3475.
Hanna, E., Fettweis, X., Mernild, S.H., Cappelen, J., Ribergaard, M.H., Shuman, C.A., Steffen, K., Wood, L., Mote, T.L., 2014. Atmospheric and oceanic climate forcing of the exceptional Greenland ice sheet surface melt in summer 2012. Int. J. Climatol. 34, 1022–1037. https://doi.org/10.1002/joc.3743.
Henderson, G.R., Barrett, B.S., Lois, A., Elsaawy, H., 2018. Time-lagged response of the antarctic and high-latitude atmosphere to tropical mjo convection. Mon. Weather Rev. 146, 1219–1231.
Henderson, G.R., Barrett, B.S., Wachowicz, L.J., Mattingly, K.S., Preece, J.R., Mote, T.L., 2021. Local and remote atmospheric circulation drivers of arctic change: a review. Front. Earth Sci. 9, 709896.
Hersbach, H., Bell, B., Berrisford, P., et al., 2020. The ERA5 global reanalysis. Q. J. R. Meteorol. Soc. https://doi.org/10.1002/qj.3803.
Jones, M.E., Bromwich, D.H., Nicolas, J.P., Carrasco, J., Plavcová, E., Zou, X., Wang, S. H., 2019. Sixty years of widespread warming in the southern middle and high latitudes (1957–2016). J. Clim. 32, 6875–6898. https://doi.org/10.1175/JCLI-D-18-0565.1.
Kittel, C., Amory, C., Hofer, S., Agosta, C., Jourdain, N.C., Gilbert, E., Toumelin, L., Vignon, E., Gallée, H., Fettweis, X., 2022. Clouds drive differences in future surface melt over the Antarctic ice shelves. Cryosphere 16, 2655–2669. https://doi.org/10.5194/tc-16-2655-2022.
Laffin, M.K., Zender, C.S., van Wessem, M., Marinsek, S., 2022. The role of foehn winds in eastern Antarctic peninsula rapid ice shelf collapse. Cryosphere 16, 1369–1381. https://doi.org/10.5194/tc-16-1369-2022.
Lee, D., Ahn, J., 2016. Future change in the frequency and intensity of wintertime North Pacific blocking in CMIP5 models. Int. J. Climatol. 37, 2765–2781. https://doi.org/10.1002/joc.4878.
Liu, P., Reed, K.A., Garner, S.T., Zhao, M., Zhu, Y., 2022. Blocking simulations in GFDL GCMs for CMIP6 and CMIP6. J. Clim. 35, 5053–5070. https://doi.org/10.1175/JCLI-D-21-0456.1.
Lu, H., Orr, A., King, J., Phillips, T., Gilbert, E., Colwell, S., Bracegirdle, T., 2023. Extreme warm events in the South Orkney Islands, Southern Ocean: compounding influence of atmospheric rivers and foehn conditions. Quart. J. Roy. Meteor. Soc. 149, 3645–3668. https://doi.org/10.1002/qj.4578.
Maclennan, M.L., Lenaerts, J.T.M., Shields, C.A., Hoffman, A.O., Wever, N., et al., 2023. Climatology and surface impacts of atmospheric rivers on West Antarctica. Cryosphere 17, 865–881. https://doi.org/10.5194/tc-17-865-2023.
Marín, J.C., Bozkurt, D., Barrett, B.S., 2022. Atmospheric blocking trends and seasonality around the Antarctic Peninsula. J. Clim. 35, 3803–3818. https://doi.org/10.1175/JCLI-D-21-0323.1.
Marshall, G.J., 2007. Half-century seasonal relationships between the southern annular mode and Antarctic temperatures. Int. J. Climatol. 27, 373–383.
Marshall, G.J., Orr, A., van Lipzig, N.P.M., King, J.C., 2006. The impact of a changing southern hemisphere annular mode on Antarctic peninsula summer temperatures. J. Clim. 19, 5388–5404. https://doi.org/10.1175/JCLI3844.1.
Masato, G., Woollings, T., Hoskins, B.J., 2014. Structure and impact of atmospheric blocking over the euro-Atlantic region in present-day and future simulations. Geophys. Res. Lett. 41, 1051–1058. https://doi.org/10.1002/2013gl058570.
Meehl, G.A., Arblaster, J.M., Bitz, C.M., Chung, C.T.Y., Teng, H., 2016. Antarctic Sea-ice expansion between 2000 and 2014 driven by tropical Pacific decadal climate variability. Nat. Geosci. 9, 590–595. https://doi.org/10.1038/ngeo2751.
Oliva, M., Navarro, F., Hrbáček, F., Hernandéz, A., Nỳvlt, D., Pereira, P., Ruiz-Fernandéz, J., Trigo, R., 2017. Recent regional climate cooling on the Antarctic peninsula and associated impacts on the cryosphere. Sci. Total Environ. 580, 210–223. https://doi.org/10.1016/j.scitotenv.2016.12.030.
Parker, T.J., Berry, G.J., Reeder, M.J., 2014. The structure and evolution of heatwaves over southeastern Australia. J. Clim. 27, 5768–5785. https://doi.org/10.1175/JCLI-D-13-00740.1.
Parsons, S., Renwick, J.A., McDonald, A.J., 2016. An assessment of future southern hemisphere blocking using CMIP5 projections from four GCMs. J. Clim. 29, 7599–7611. https://doi.org/10.1175/JCLI-D-15-0754.1.
Pezza, A.B., Durrant, T., Simmonds, I., Smith, I., 2008. Southern hemisphere synoptic behavior in extreme phases of SAM, ENSO, sea ice extent, and southern Australia rainfall. J. Clim. 21, 5566–5584. https://doi.org/10.1175/2008JCLI2128.1.

Pohl, B., Favier, V., Wille, J., Udy, D.G., Vance, T.R., et al., 2021. Relationship between weather regimes and atmospheric rivers in East Antarctica. J. Geophys. Res. Atmos. 126, e2021JD035294 https://doi.org/10.1029/2021JD035294.

Rignot, E., Mouginot, J., Scheuchl, B., van den Broeke, M., van Wessem, M.J., Morlighem, M., 2019. Four decades of Antarctic ice sheet mass balance from 1979-2017. P. Natl. Acad. Sci. 116, 1095–1103. https://doi.org/10.1073/pnas.1812883116.

Rodrigues, R.R., Woollings, T., 2017. Impact of atmospheric blocking on South America in austral summer. J. Clim. 30, 1821–1837. https://doi.org/10.1175/JCLI-D-16-0493.1.

Rodrigues, R.R., Taschetto, A.S., Sen Gupta, A., et al., 2019. Common cause for severe droughts in South America and marine heatwaves in the South Atlantic. Nat. Geosci. 12, 620–626. https://doi.org/10.1038/s41561-019-0393-8.

Rondanelli, R., Hatchett, B., Rutllant, J., Bozkurt, D., Garreuad, R., 2019. Strongest MJO on record triggers extreme Atacama rainfall and warmth in Antarctica. Geophys. Res. Lett. 46, 3482–3491. https://doi.org/10.1029/2018GL081475.

Scambos, T.A., Bohlander, J.A., Human, C.A., Skvarca, P., 2004. Glacier acceleration and thinning after ice shelf collapse in the Larsen B embayment. Geophys. Res. Lett. 31, L18402. https://doi.org/10.1029/2004GL020670.

Schaller, N., Sillmann, J., Anstey, J., Fischer, E.M., Grams, C.M., Russo, S., 2018. Influence of blocking on northern European and Western Russian heatwaves in large climate model ensembles. Environ. Res. Lett. 13, 054015 https://doi.org/10.1088/1748-9326/aaba55.

Siegert, M.J., Atkinson, A., Banwell, A., Brandon, M., Convey, P., Davies, B., et al., 2019. The Antarctic peninsula under a 1.5°c global warming scenario. Front. Environ. Sci. 7 https://doi.org/10.3389/fenvs.2019.00102.

Siegert, M.J., Bentley, M.J., Atkinson, A., Bracegirdle, T.J., Convey, P., Davies, B., et al., 2023. Antarctic extreme events. Front. Environ. Sci. 11 https://doi.org/10.3389/fenvs.2023.1229283.

Sousa, P.M., Trigo, R.M., Barriopedro, D., Soares, P.M., Santos, J.A., 2018. European temperature responses to blocking and ridge regional patterns. Clim. Dyn. 50, 457–477. https://doi.org/10.1007/s00382-017-3620-2.

Steig, E.J., Ding, Q., Battisti, D., Jenkins, A., 2012. Tropical forcing of circumpolar deep water inflow and outlet glacier thinning in the Amundsen Sea embayment, West Antarctica. Ann. Glaciol. 53, 19–28.

Tri Datta, R., Tedesco, M., Fettweis, X., Agosta, C., Lhermitte, S., Lenaerts, J.T.M., 2019. The effect of foehn-induced surface melt on firn evolution over the Northeast Antarctic peninsula. Geophys. Res. Lett. 46, 3822–3831. https://doi.org/10.1029/2018GL080845.

Turner, J., Lu, H., White, I., King, J.C., Phillips, T., Hosking, J.S., Bracegirdle, T.J., Marshall, G.J., Mulvaney, R., Deb, P., 2016. Absence of 21st century warming on Antarctic peninsula consistent with natural variability. Nature 535, 411–415. https://doi.org/10.1038/nature18645.

Turner, J., Lu, H., King, J., Marshall, G.J., Phillips, T., Bannister, D., Colwell, S., 2021. Extreme temperatures in the Antarctic. J. Clim. 34, 2653–2668. https://doi.org/10.1175/JCLI-D-20-0538.1.

Turton, J.V., Kirchgaessner, A., Ross, A.N., King, J.C., Kuipers-Munneke, P., 2020. The influence of foehn winds on annual and seasonal surface melt on the Larsen C Ice Shelf, Antarctica. Cryosphere 14, 4165–4180. https://doi.org/10.5194/tc-14-4165-2020.

Wachowicz, L.J., Preece, J.R., Mote, T.L., Barrett, B.S., Henderson, G.R., 2021. Historical trends of seasonal Greenland blocking under different blocking metrics. Int. J. Climatol. 41, E3263–E3278. https://doi.org/10.1002/joc.6923.

Wille, J., Favier, V., Jourdain, N.C., Kittel, C., Turton, J.V., Agosta, C., Gorodetskaya, I. V., Picard, G., Codron, F., Leroy-Dos Santos, C., Amory, C., Fettweis, X., Blanchet, J., Jomelli, V., Berchet, A., 2022. Intense atmospheric rivers can weaken ice shelf stability at the Antarctic peninsula. Commun. Earth Environ. 3, 90. https://doi.org/10.1038/s43247-022-00422-9.

Wille, J.D., Favier, V., Gorodetskaya, I.V., Agosta, C., Kittel, C., Beeman, J.C., Jourdain, N.C., Lenaerts, J.T., Codron, F., 2021. Antarctic atmospheric river climatology and precipitation impacts. J. Geophys. Res. Atmos. 126, e2020JD033788 https://doi.org/10.1029/2020JD033788.

Wille, J.D., Alexander, S.P., Amory, C., Baiman, R., et al., 2024. The extraordinary march 2022 east antarctica "heat" wave. part i: observations and meteorological drivers. J. Clim. 37, 757–778. https://doi.org/10.1175/JCLI-D-23-0175.1.

Woods, C., Caballero, R., Svensson, G., 2013. Large-scale circulation associated with moisture intrusions into the arctic during winter. Geophys. Res. Lett. 40, 4717–4721. https://doi.org/10.1002/grl.50912.

Woollings, T., Barriopedro, D., Methven, J., Son, S.W., Martius, O., Harvey, B., Sillmann, J., Lupo, A.R., Seneviratne, S., 2018. Blocking and its response to climate change. Curr. Clim. Chang. Rep. 4, 287–300. https://doi.org/10.1007/s40641-018-0108-z.

Xu, M., Yu, L., Liang, K., Vihma, T., Bozkurt, D., Hu, X., Yang, Q., 2021. Dominant role of vertical air flows in the unprecedented warming on the Antarctic peninsula in February 2020. Commun. Earth Environ. 2, 133. https://doi.org/10.1038/s43247-021-00203-w.

Yuan, X., Martinson, D.G., 2001. The antarctic dipole and its predictability. Geophys. Res. Lett. 28, 3609–3612.

Yuan, X., Kaplan, M.R., Cane, M.A., 2018. The interconnected global climate system-a review of tropical-polar teleconnections. J. Clim. 31, 5765–5792. https://doi.org/10.1175/JCLI-D-16-0637.1.

Zhu, J., Xie, A., Qin, X., Wang, S., Xu, B., Wang, Y., 2023. Projection an Antarctic temperature extremes from the CMIP6 multimodal ensemble under different scenarios. J. Appl. Meteorol. Climatol. 62, 1129–1146. https://doi.org/10.1175/JAMC-D-22-0137.1.

Zou, X., Rowe, P.M., Gorodetskaya, I., Bromwich, D.H., Lazzara, M.A., Cordero, R.R., et al., 2023. Strong warming over the Antarctic peninsula during combined atmospheric river and foehn events: contribution of shortwave radiation and turbulence. J. Geophys. Res. Atmos. 128, e2022JD038138 https://doi.org/10.1029/2022JD038138.